

Finite-source and finite-lens effects in astrometric microlensing

C.-H. Lee^{1*}, S. Seitz^{1,2}, A. Riffeser¹ and R. Bender^{1,2}

¹University Observatory Munich, Scheinerstrasse 1, 81679 München, Germany

²Max Planck Institute for Extraterrestrial Physics, Giessenbachstrasse, 85748 Garching, Germany

Accepted –. Received –; in original form 2010 January 14

ABSTRACT

The aim of this paper is to study the astrometric trajectory of microlensing events with an extended lens and/or source. We consider not only a dark lens but also a luminous lens as well. We find that the discontinuous finite-lens trajectories given by Takahashi will become continuous in the finite-source regime. The point lens (source) approximation alone gives an under (over)estimation of the astrometric signal when the size of the lens and source are not negligible. While the finiteness of the source is revealed when the lens transits the surface of the source, the finite-lens signal is most prominent when the lens is very close to the source. Astrometric microlensing towards the Galactic bulge, Small Magellanic Cloud and M31 are discussed, which indicate that the finite-lens effect is beyond the detection limit of current instruments. Nevertheless, it is possible to distinguish between self-lensing and halo lensing through a (non-)detection of the astrometric ellipse. We also consider the case where the lens is luminous itself, as has been observed where a lensing event was followed up with the *Hubble Space Telescope*. We show that the astrometric signal will be reduced in a luminous-lens scenario. The physical properties of the event, such as the lens-source flux ratio, the size of the lens and source nevertheless can be derived by fitting the astrometric trajectory.

Key words: gravitational lensing: micro – astrometry – dark matter.

1 INTRODUCTION

Most of the microlensing events detected to date are through photometric monitoring of the source flux. In this case, the information on the physical identity of the lens is reduced, because the only quantity one can retrieve from the light curve is the Einstein timescale t_E . t_E is defined by the time required for the source to transit the angular Einstein radius θ_E of the lens (Gould 2000):

$$t_E = \frac{\theta_E}{|\mu_{rel}|}, \quad \theta_E = \sqrt{k M_L \pi_{rel}}, \quad k \equiv \frac{4G}{c^2 \text{AU}} \approx 8.14 \frac{\text{mas}}{M_\odot}, \quad (1)$$

where μ_{rel} is the relative lens-source proper motion, M_L is the mass of the lens, $\pi_{rel} := \text{AU}/(D_{OL}^{-1} - D_{OS}^{-1})$ is the relative lens-source parallax, D_{OL} and D_{OS} are distance to the lens and the source from the observer, respectively. Equation (1) shows that the mass, distance, and velocity of the lens are degenerated into t_E .

To better constrain the lens properties, Hog, Novikov, & Polnarev (1995), Walker (1995) and Miyamoto & Yoshii (1995) thus suggested to use astrometric microlensing. That is, to measure the centroid displacement of the two images during the course of microlensing. Former studies have shown that the trajectory of the centroid displacement will trace out an ellipse, and the size of the ellipse is proportional to the angular Einstein radius. Therefore, one can determine θ_E through the observation of such astrometric ellipses and constrain the relative

lens-source proper motion. Gould (1992) has shown that if one can further measure the microlens parallax $\pi_E = \sqrt{\pi_{rel}/(k M_L)}$ form the light-curve distortion induced by the orbital motion of the Earth, the lens mass M_L and the relative lens-source parallax π_{rel} can be determined without ambiguity:

$$M_L = \frac{\theta_E}{k \pi_E}, \quad \pi_{rel} = \pi_E \theta_E. \quad (2)$$

The location of the lens can be derived as well if the distance to the source is well known, which is often the case towards the Galactic bulge and Magellanic Clouds.

The typical value of the astrometric microlensing signal for a source in the Galactic bulge and a $0.5 M_\odot$ lens located half-way to the source is of order of 0.1 mas, which is much larger than the astrometric accuracy of upcoming space missions such as *Space Interferometry Mission* (*SIM*; Allen, Peterson, & Shao 1997), *Global Astrometric Interferometer for Astrophysics* (*GAIA*; Lindegren et al. 1994) and ground-based instruments, e.g. *Phase Referenced Imaging and Micro-arcsecond Astrometry* (*PRIMA*; Quirrenbach et al. 1998). *GAIA* will survey the whole sky with sources brighter than 20 mag in *V* band. It is expected to reach an astrometric accuracy of 30 μas (150 μas) with $V < 12$ ($V < 16$) for a single measurement (Belokurov & Evans 2002) and an estimated detection of ≈ 1000 events (Dominik & Sahu 2000). Unlike *GAIA*, which only scans the sky with a pre-determined pattern, *SIM* can point to selectable targets and thus tracks the ongoing microlensing event upon request. The expected accuracy of *SIM* is 5 μas (20 μas)

* E-mail: chlee@usm.lmu.de

for $V < 12$ ($V < 16$) with 1-hour integration time (Goullioud et al. 2008). While *SIM* and *GAIA* are scheduled to launch in the next few years, *PRIMA* has already been installed on the Very Large Telescope Interferometer (VLTI) and aims at achieving 10- μ as accuracy level in 30 min integration time provided a reference star within 10 arcsec and a 200-m baseline (Delplancke 2008).

In addition to the standard point-source point-lens (PSPL) microlensing, single-lens events revealing an extended source signal have also been observed photometrically (e.g. Alcock et al. 1997b; Jiang et al. 2004; Yoo et al. 2004; Cassan et al. 2006; Batista et al. 2009; Yee et al. 2009; Zub et al. 2009; Fouqué et al. 2010). Mao & Witt (1998) thus derived the astrometric trajectory of finite-source events with a point-lens (FSPL). On the other hand, Takahashi (2003) studied the centroid displacement of finite-lens effects but assuming a point-source (PSFL). Furthermore, Agol (2002) and Lee et al. (2009) have investigated the combination of finite-source and finite-lens (FSFL) effects photometrically, but left aside the astrometric aspect. Since the FSFL light curve deviates from either the PSFL or FSPL, as shown by Agol (2002), we are motivated to study the astrometric behaviour when both FS and FL effects are relevant. There are events where both the source and the lens are resolved by the *Hubble Space Telescope* (*HST*). This implies that the lens can also be a star and implies a luminous-lens scenario rather than a dark lens (Alcock et al. 2001; Kozłowski et al. 2007), which is also the case for self-lensing. We thus consider the light contribution from the lens star and study the astrometric behaviour by allowing for a luminous lens.

This paper is organized as follows. In § 2 we introduce the theory of astrometric microlensing. We take into account the FS effects either with a uniform surface brightness source or with a more general surface brightness profile in § 3. We further include a dark lens with finite size in § 4. One might expect not only shadowing but also light contribution from the lens as well. Therefore, we allow for a luminous lens in § 5. The aforementioned properties of the microlensing system can be estimated by fitting the formula in § 5. A discussion of possible events with sources located in the Galactic bulge, Small Magellanic Cloud (SMC) and M31 is presented in § 6 followed by a summary in § 7.

2 ASTROMETRIC TRAJECTORY OF THE LENSED IMAGES

Let φ_s and φ_L be the angular position of the source and lens. Then one can derive the position (θ) and the amplification (A) of the two lensed images in the lens plane through the dimensionless impact parameter $u := (\varphi_s - \varphi_L)/\theta_E$ (see e.g. Hosokawa et al. 1993; Hog, Novikov, & Polnarev 1995; Walker 1995; Miyamoto & Yoshii 1995):

$$\theta_{\pm} = \frac{1}{2} \left[u \pm \sqrt{u^2 + 4} \right] \hat{u}, \quad A_{\pm} = \frac{1}{2} \left[\frac{u^2 + 2}{u\sqrt{u^2 + 4}} \pm 1 \right], \quad (3)$$

where $u = |\mathbf{u}|$ and $\hat{u} = \mathbf{u}/u$. Note that θ_{\pm} and \hat{u} are vectors while A_{\pm} are scalars. The centroid of the images can be calculated by weighting the position of the two images with their amplification:

$$\theta_{c,PSPL} = \frac{A_+ \theta_+ + A_- \theta_-}{A_+ + A_-} = \frac{1}{2} \left[\frac{u(u^2 + 4)}{u^2 + 2} + u \right] \hat{u} \quad (4)$$

and the centroidal shift relative to the source is

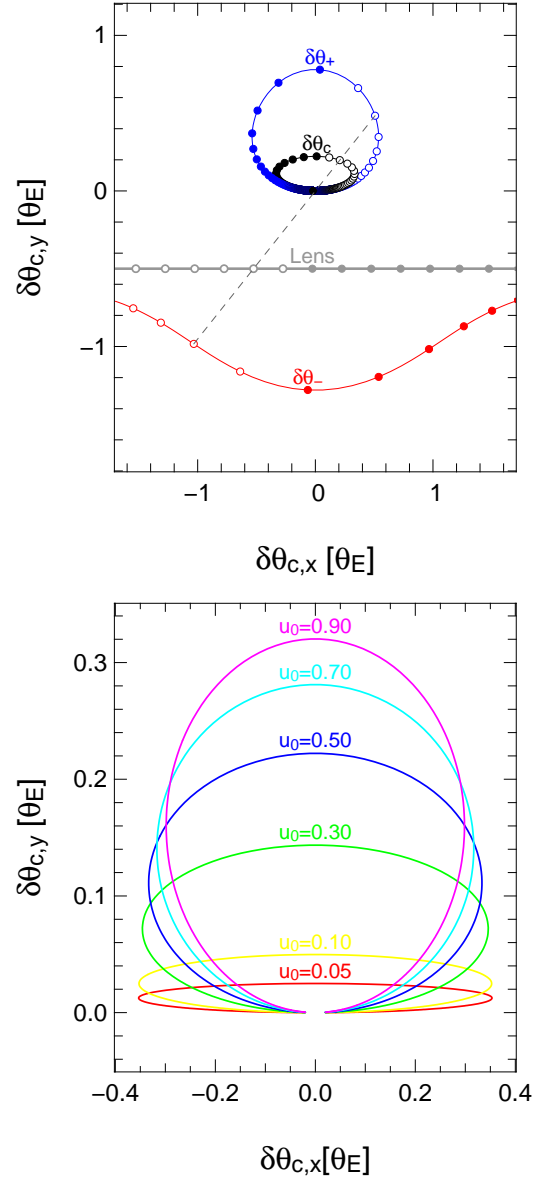


Figure 1. Centroid shifts for PSPL. Upper panel: the trajectory of the plus-image (in blue), minus-image (in red), centroid of these two images (in black), and the lens (in gray) relative to the source center assuming $t_0 = 0$, $t_E = 10$ d, and $u_0 = 0.5 \theta_E$. Lower panel: centroid displacement for different values of u_0 .

$$\delta\theta_{c,PSPL} = \theta_c - \mathbf{u} = \frac{u}{u^2 + 2} \hat{u}. \quad (5)$$

If we neglect the parallax effects, the relative motion between the lens and source can be approximated by rectilinear motion so that

$$u(t) = \sqrt{\tau^2 + u_0^2}, \quad \tau = \frac{t - t_0}{t_E}, \quad (6)$$

where u_0 is the closest approach at t_0 .

The centroidal shift can then be decomposed into components parallel to $\boldsymbol{\mu}_{rel}$, $\delta\theta_{c,PSPL,x}$, and perpendicular to $\boldsymbol{\mu}_{rel}$, $\delta\theta_{c,PSPL,y}$ (see Fig. 1). One further finds that the centroidal shift actually traces out an ellipse (Walker 1995)

$$\left(\frac{\delta\theta_{c,PSPL,x}}{a} \right)^2 + \left(\frac{\delta\theta_{c,PSPL,y} - b}{b} \right)^2 = 1, \quad (7)$$

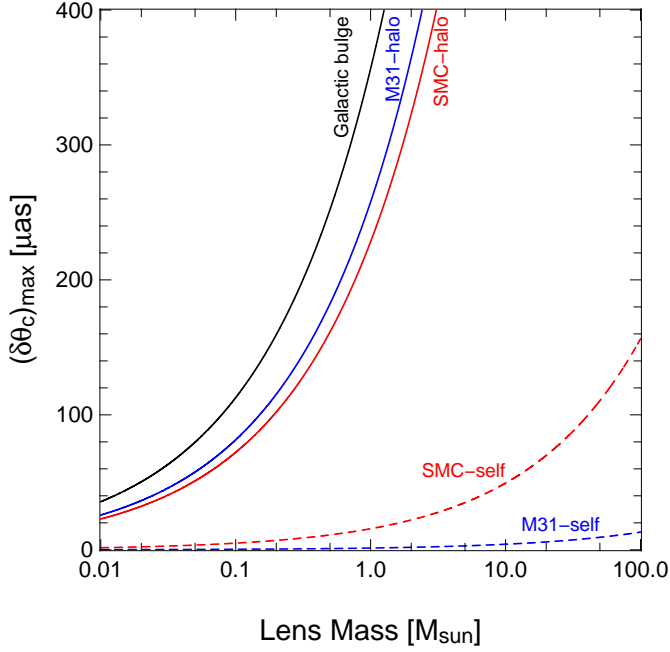


Figure 2. Maximum values for the centroidal shift versus lens mass. For illustration, we set the lens of halo lensing towards SMC ($D_{\text{OS}} = 65$ kpc) and M31 ($D_{\text{OS}} = 770$ kpc) to be 15 kpc from the observer, and 1 kpc in front of the source as self-lensing. We only show the case of halo lensing for Galactic bulge ($D_{\text{OS}} = 8$ kpc) assuming the lens is half-way to the background source.

where a and b are the semi-major and semi-minor axis of the ellipse, respectively,

$$a = \frac{1}{2} \frac{1}{\sqrt{u_0^2 + 2}}, \quad b = \frac{1}{2} \frac{u_0}{u_0^2 + 2}. \quad (8)$$

The trajectory of centroidal shift with different values of u_0 is shown in Fig. 1.

Taking the derivative of equation (5), one finds that the maximum centroidal shift occurs when $u = \sqrt{2}$ and has an absolute value of $\sqrt{2}/(2+2) = 1/(2\sqrt{2}) \approx 0.3536$, i.e. about one-third of the angular Einstein radius. For a source located in the Galactic bulge with a lens of $0.5 M_\odot$ located half-way to the source, the angular Einstein radius is $712 \mu\text{as}$, which is 1 (2) mag larger than the planned astrometric accuracy of the *GAIA* (*SIM*) mission even after taking one-third of its value. The maximum values for the centroidal shifts with halo and self-lensing towards SMC and M31 are shown in Fig. 2.

3 THE FINITE-SOURCE EFFECTS

For an extended source, the centroid of the two images is obtained by a two-dimensional integral of the image position weighted by its amplification over the surface of the source (Walker 1995; Mao & Witt 1998):

$$\delta\theta_{c,\text{FSPL}} = \frac{\int_0^{2\pi} \int_0^{\rho_S} [A_+ \theta_+ + A_- \theta_-] S\left(\frac{r}{\rho_S}\right) r dr d\phi}{\int_0^{2\pi} \int_0^{\rho_S} [A_+ + A_-] S\left(\frac{r}{\rho_S}\right) r dr d\phi} - \mathbf{u} \quad (9)$$

where $S(\frac{r}{\rho_S})$ is the source surface-brightness profile, $\rho_S := \theta_S/\theta_E$ is the source radius in units of the angular Einstein ring

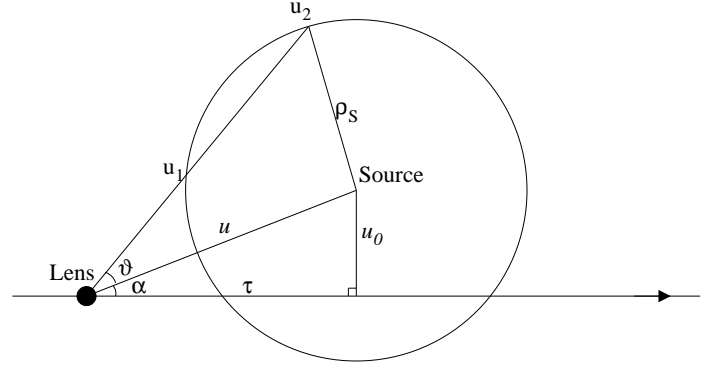


Figure 3. Schematic view of the lens-centered coordinates used in equation (10).

radius and r is the distance to the source centre.

For a source with uniform surface brightness [i.e. $S(\frac{r}{\rho_S})$ is constant all over the surface of the source], the integration over the source surface can be reduced into a one-dimensional integral following the lens-centered coordinates approach of Lee et al. (2009). One thus derives the values for $\delta\theta_{c,\text{FSPL},x}$ and $\delta\theta_{c,\text{FSPL},y}$

$$\begin{aligned} \delta\theta_{c,\text{FSPL},x} &= \frac{\int_0^{2\pi} \left[\frac{1}{3} (\tilde{u}^2 + 1) \sqrt{\tilde{u}^2 + 4} \right]_{\tilde{u}=u_1}^{u_2} \cos(\vartheta + \alpha) d\vartheta}{\int_0^{2\pi} \left[\frac{1}{2} \tilde{u} \sqrt{\tilde{u}^2 + 4} \right]_{\tilde{u}=u_1}^{u_2} d\vartheta} - \tau, \\ \delta\theta_{c,\text{FSPL},y} &= \frac{\int_0^{2\pi} \left[\frac{1}{3} (\tilde{u}^2 + 1) \sqrt{\tilde{u}^2 + 4} \right]_{\tilde{u}=u_1}^{u_2} \sin(\vartheta + \alpha) d\vartheta}{\int_0^{2\pi} \left[\frac{1}{2} \tilde{u} \sqrt{\tilde{u}^2 + 4} \right]_{\tilde{u}=u_1}^{u_2} d\vartheta} - u_0, \end{aligned} \quad (10)$$

where the integration boundaries u_1 and u_2 are

$$\begin{aligned} u_1 &= \begin{cases} 0 & u \leq \rho_S \\ u \cos \vartheta - \sqrt{\rho_S^2 - u^2 \sin^2 \vartheta} & u > \rho_S \wedge \vartheta \leq \sin^{-1}(\frac{\rho_S}{u}) \\ 0 & u > \rho_S \wedge \vartheta > \sin^{-1}(\frac{\rho_S}{u}) \end{cases} \\ u_2 &= \begin{cases} u \cos \vartheta + \sqrt{\rho_S^2 - u^2 \sin^2 \vartheta} & u \leq \rho_S \\ u \cos \vartheta + \sqrt{\rho_S^2 - u^2 \sin^2 \vartheta} & u > \rho_S \wedge \vartheta \leq \sin^{-1}(\frac{\rho_S}{u}) \\ 0 & u > \rho_S \wedge \vartheta > \sin^{-1}(\frac{\rho_S}{u}) \end{cases} \end{aligned} \quad (11)$$

and $\alpha = \tan^{-1}(u_0/\tau)$. The relative lens-source configuration and the parameters used in equations (10)-(11) are sketched in Fig. 3.

An example for an FS centroidal shift is shown in Fig. 4 along with the light curve in Fig. 5. The FS effect drives the centroidal shift towards the source center for small u , and the trajectory becomes cloverleaf-like when u_0 is smaller than the source radius (see Fig. 7).

We also show the centroidal shifts of a limb-darkened source with an one parameter linear limb-darkening profile (Yoo et al. 2004), that is

$$S\left(\frac{r}{\rho_S}\right) = \bar{S} \left[1 - \Gamma_S \left(1 - \frac{3}{2} \sqrt{1 - \left(\frac{r}{\rho_S}\right)^2} \right) \right], \quad (12)$$

where r is the distance to the source center. Γ_S is the wavelength-dependent limb-darkening coefficient. \bar{S} is the mean surface brightness of the source. When $\Gamma_S = 0$, equation (12) gives us a source with uniform brightness. The trajectory of the centroidal shift by the limb-darkened sources shows only small difference from that of the uniform brightness source, as shown in Figs 6 and 7.

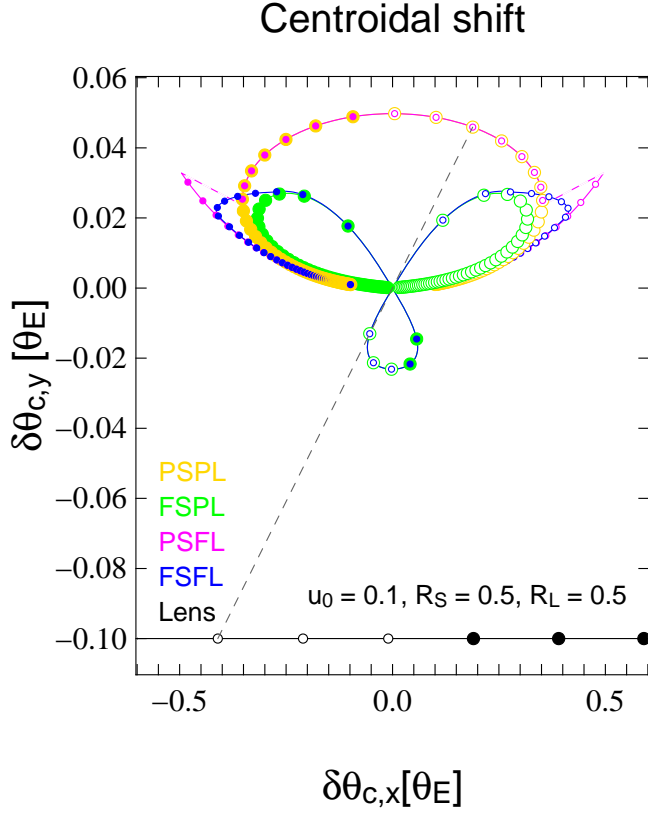


Figure 4. An example for centroidal shifts of a microlensing event assuming $u_0 = 0.1 \theta_E$, source radius $= 0.5 \theta_E$ and lens radius $= 0.5 \theta_E$. We show the trajectory of a PSPL (in yellow), FSPL (in green), PSFL (in red), and FSFL (in blue). Note that the dashed red line indicates the discontinuous part of the trajectory in a PSFL event.

4 THE FINITE-LENS EFFECTS

For simplicity, we begin with the case of PSFL. The light from the plus-image will be obscured by the lens if its distance to the lens is smaller than the lens radius. That is, the plus-image vanishes when $\theta_+ = |\theta_+| < \rho_L$ ($\rho_L := \theta_L/\theta_E$). Similarly, the minus-image vanishes when $\theta_- = |\theta_-| < \rho_L$. Therefore, the centroidal shift taking into account the lens size is (Takahashi 2003)

$$\delta\theta_{c,\text{PSFL}} = \frac{A_+ \theta_+ \Theta(\theta_+ - \rho_L) + A_- \theta_- \Theta(\theta_- - \rho_L)}{A_+ \Theta(\theta_+ - \rho_L) + A_- \Theta(\theta_- - \rho_L)} - u, \quad (13)$$

where $\Theta(x)$ is the Heaviside step function. An example for a PSFL centroidal shift is shown in Fig. 4 along with the light curve in Fig. 5. The trajectory is composed of two discontinuous parts: it follows the plus-image trajectory at larger u and returns to the PSPL centroidal trajectory at smaller u . This can be explained as follows. When the FL effects set in, the lens first obscures the minus-image because it is always inside the Einstein ring and has smaller distance to the lens compared to the plus-image (which is always outside the Einstein ring). In addition, the value of θ_- becomes larger for smaller u , as we can see from Fig. 1, which brings the trajectory back to the PSPL centroidal trajectory at smaller u for smaller ρ_L . As a consequence, when the size of the lens increases, the trajectory tends to be more plus-image-like until the lens size becomes so large that it completely obscures the light even from the plus-image.

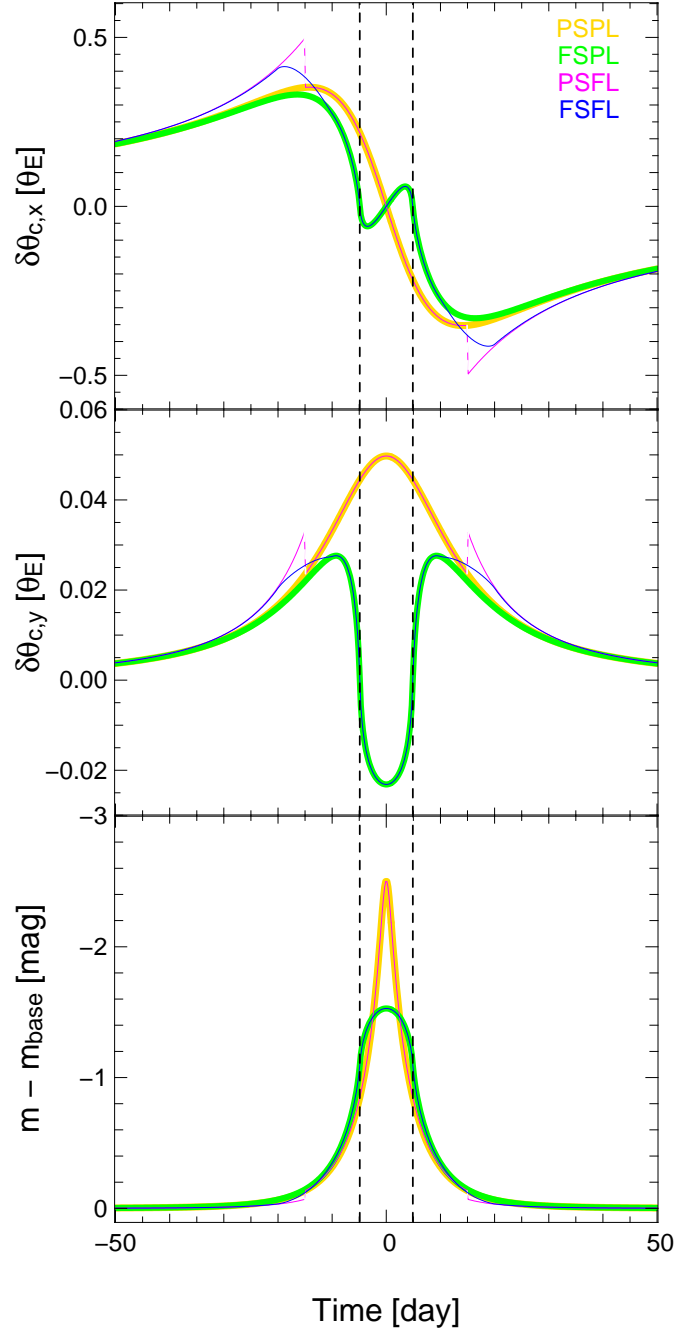


Figure 5. Centroidal shifts decomposition and light curves of a microlensing event assuming $u_0 = 0.1 \theta_E$, source radius $= 0.5 \theta_E$ and lens radius $= 0.5 \theta_E$. We show the trajectory in the x- and y-direction (as in Fig. 1) of a PSPL (in yellow), FSPL (in green), PSFL (in red), and FSFL (in blue). We also show the light curve with the magnitude variation relative to the baseline (m_{base}). The vertical dashed line indicates the time when $u_0 = \rho_S$. Note that the discontinuous part of the trajectory in a PSFL event is indicated by the dashed red line.

Combining equations (9) and (13), we are able to fully consider the FSFL effects:

$$\delta\theta_{c,\text{FSFL}} = \frac{\int_0^{2\pi} \int_0^{\rho_S} [A_+ \theta_+ \Theta(\theta_+ - \rho_L) + A_- \theta_- \Theta(\theta_- - \rho_L)] S\left(\frac{r}{\rho_S}\right) r dr d\phi}{\int_0^{2\pi} \int_0^{\rho_S} [A_+ \Theta(\theta_+ - \rho_L) + A_- \Theta(\theta_- - \rho_L)] S\left(\frac{r}{\rho_S}\right) r dr d\phi} - u. \quad (14)$$

The result is again shown in Fig. 4 along with the light curve. The trajectory first follows the PSFL trajectory at larger u , but, instead of a discontinuous jump, the FS effects is now bending the trajectory towards the FSPL trajectory until it fully becomes the FSPL trajectory at small u .

To illustrate the importance of simultaneously including the finiteness of both the lens and the source, we compare $\delta\theta_{c,x}$ and $\delta\theta_{c,y}$ for the cases of PSPL, FSPL, PSFL, and FSFL in Fig. 5. When the size of the lens and the source are both negligible, it is clear that one would overestimate $\delta\theta_c$ by adopting the PS approximation. On the other hand, taking the PL assumption would underestimate the value of $\delta\theta_c$. Another important point is that in the FSFL scenario, one cannot determine the lens size by measuring the discontinuities in the trajectory presented by Takahashi (2003) because the FS effect makes the trajectory continuous. One thus needs to use equation (14) for deriving both ρ_L and ρ_S .

We also show how the limb darkening changes the centroidal shift on top of a FSFL event (see Fig. 6) assuming different values of the limb-darkening coefficient Γ_S . In general, the limb-darkening only slightly modifies the astrometric trajectory. The FS effects and the limb darkening are most prominent when the lens transits the surface of the source, as indicated in Figs 5 and 6.

By fitting the centroidal shifts and/or the light curve as presented in Figs 5 and 6, one is able to constrain the value of ρ_S , ρ_L and the limb-darkening coefficient Γ_S . Events exhibiting FS effects have been detected photometrically (e.g. Alcock et al. 1997b; Jiang et al. 2004; Yoo et al. 2004; Cassan et al. 2006; Batista et al. 2009; Yee et al. 2009; Zub et al. 2009; Fouqué et al. 2010), and the information of ρ_S and Γ_S has been retrieved by fitting the light curve. Although it is hard to tell the difference between the FS and PS light curve by eye inspection, including the FS effects actually dramatically reduces the χ^2 value for the best-fitted parameters. One can further fit the limb-darkening coefficient in different wavelength on top of the FS effects if multiwavelength observations are available. Practically, the limb darkening is relevant when one wants to simultaneously fit photometric observations from different bands. However, one cannot measure the value of θ_E directly from the light curve and thus the information of the actual source size is unknown. Albrow et al. (2000) suggested to deal with this problem in the other way around. That is, given the colour information of the source by photometric observation, one can apply the relation between the colour and the surface brightness to obtain the actual source size if the stellar type of the source is known from the spectroscopic observation. Then the value of θ_E can be calculated by $\theta_E := \theta_S / \rho_S$. Constraints on the lens mass and distance are also possible given the information of microlens parallax π_E . However, inferring θ_E photometrically from the source size is achievable only if the FS effect can be seen in the light curve, which is the case only when the lens transits the surface of the source, as discussed by Gould (1994).

The advantage of astrometric microlensing is that the size of the astrometric signal is proportional to the value of θ_E . This means one can potentially measure θ_E for every single event even if the FS effects in the light curve are not prominent. Given the information of θ_E , the actual size of the lens and the source are ρ_S and ρ_L multiplied by θ_E . It is also possible to compare the source size derived from the astrometric microlensing and from the colour to surface brightness relation.

We show the FSFL effects for a source of a uniform and a limb-darkened surface brightness profile with different source and lens sizes in Fig. 7 to illustrate how the combination of FS and FL influence the centroidal trajectory. The upper row of Fig. 7 gives

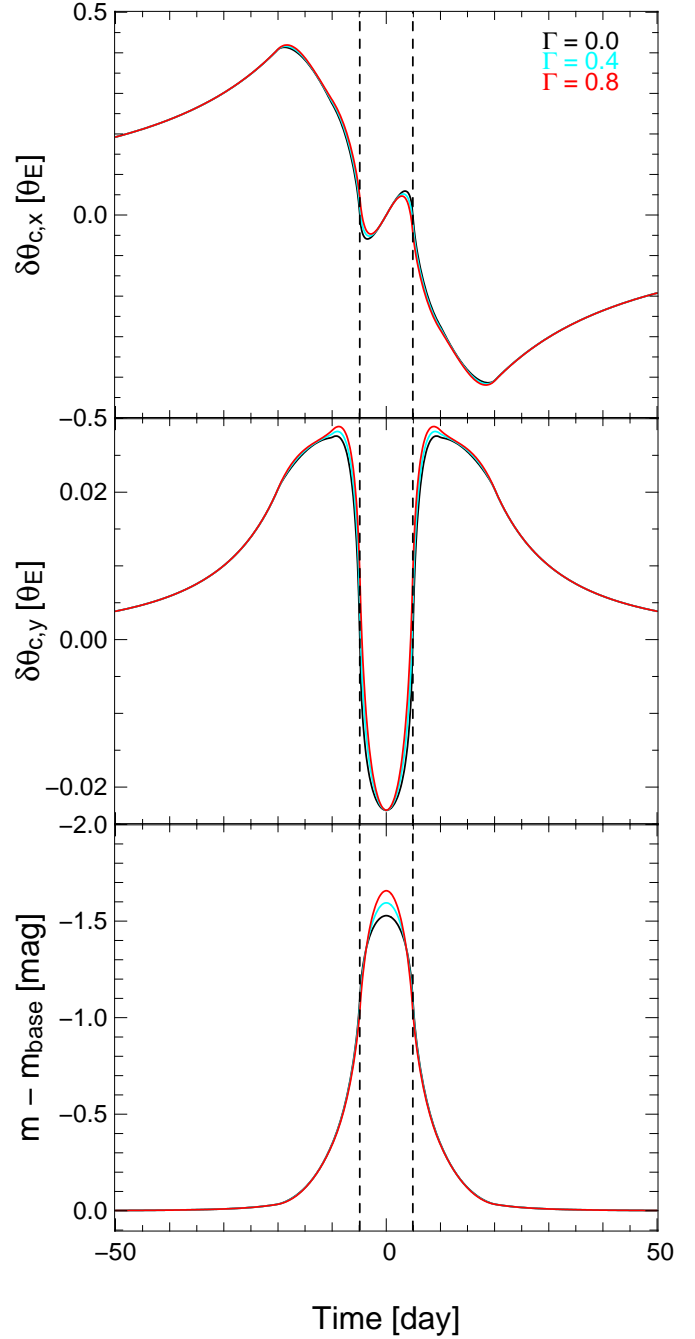


Figure 6. Centroidal shifts decomposition and light curves of a microlensing event assuming $u_0 = 0.1 \theta_E$, source radius $= 0.5 \theta_E$ and lens radius $= 0.5 \theta_E$. We show the trajectory in the x- and y-direction (as in Fig. 1) of a uniform brightness source (in black), a limb-darkened source with $\Gamma_S = 0.4$ (in cyan) and $\Gamma_S = 0.8$ (in red). We also show the light curve with the magnitude variation relative to the baseline (m_{base}). The vertical dashed line indicates the time when $u_0 = \rho_S$.

the cases of PL approximation, which are comparable to the results of Mao & Witt (1998). The left-hand column of Fig. 7 shows the cases of PS approximation comparable to the results by Takahashi (2003).

centroidal shifts of a limb-darkened source

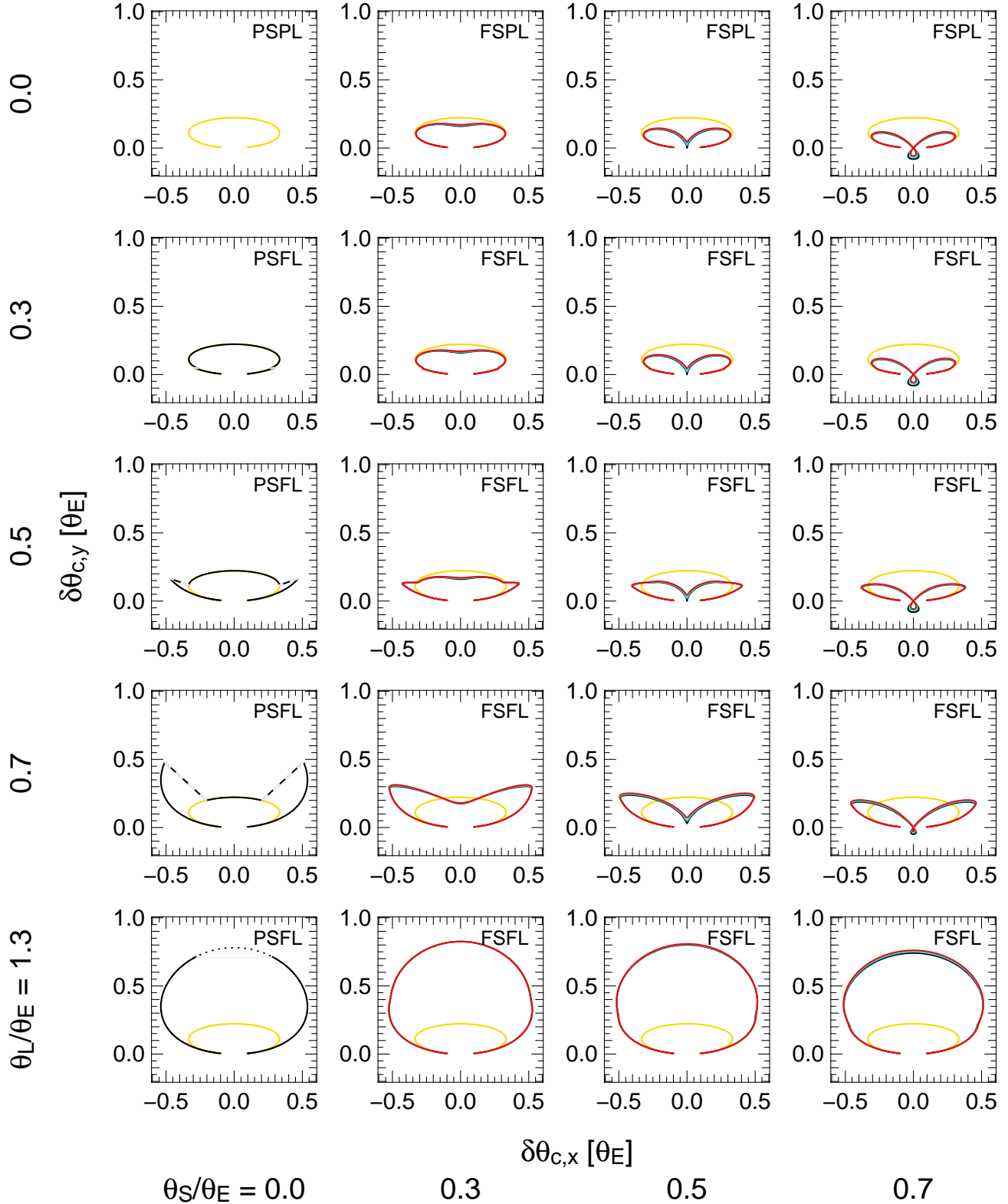


Figure 7. Centroid shifts in the presence of FS and FL effects for a dark lens. We show the examples for a PSPL (in yellow), FSFL with a uniform surface brightness source (in black) and with a limb-darkened source (in cyan: $\Gamma_S = 0.4$ and in red: $\Gamma_S = 0.8$) assuming $u_0 = 0.5 \theta_E$ and with the sizes of the source and the lens varying from $0.3 \theta_E$ to $1.3 \theta_E$. The dashed lines in the plots with $\theta_S / \theta_E = 0.0$ show the discontinuity in the trajectories for the PSFL cases. The dotted line in the PSFL with $\theta_L / \theta_E = 1.3$ indicates the trajectory when the lens totally obscures both the plus- and minus-image.

5 THE LUMINOUS-LENS EFFECTS

There are microlensing systems where both the source and the lens are resolved by *HST* (Alcock et al. 2001; Kozłowski et al. 2007). This indicates that the lens might be a luminous foreground star and thus perturbs the light centroid during the course of microlensing.

Let us now consider the case where the light contribution from the lens is not negligible and start with the simple PSPL case. When the source is lensed by a point luminous lens (PSPLL), the centroid becomes the sum of the position multiplied by the flux of the two images and the lens over the total one. Furthermore, the reference point for the centroid shift is no longer the source centre, but the flux centre between the unlensed source and the lens instead (Boden, Shao, & van Buren 1998; Jeong, Han, & Park 1999; Dominik & Sahu 2000)

$$\delta\theta_{c,PSPLL} = \frac{A_+\theta_+ + A_-\theta_- + f_{LS}\theta_L}{A_+ + A_- + f_{LS}} - \frac{\mathbf{u}}{1 + f_{LS}}, \quad (15)$$

where $f_{LS} = f_L/f_S$ is the flux ratio between the lens and source and θ_L is the position of the lens on the lens plane. Here the $f_{LS}\theta_L$ term vanishes benefiting from the advantage of the lens-centred coordinates. For the case of FSFL, one just needs to modify the first part of equation (15) by putting in the FL criteria of equation (13) and performing the integration over the source surface as equation (10) for a uniform brightness source or equation (9) for a more general source brightness profile, that is

$$\delta\theta_{c,FSFL} = \frac{\int_0^{2\pi} \int_0^{\rho_S} [A_+\theta_+ \Theta(\theta_+ - \rho_L) + A_-\theta_- \Theta(\theta_- - \rho_L)] S\left(\frac{r}{\rho_S}\right) r dr d\phi + f_{LS}\theta_L}{\int_0^{2\pi} \int_0^{\rho_S} [A_+\Theta(\theta_+ - \rho_L) + A_-\Theta(\theta_- - \rho_L)] S\left(\frac{r}{\rho_S}\right) r dr d\phi + f_{LS}} - \frac{\mathbf{u}}{1 + f_{LS}}. \quad (16)$$

Here we illustrate the influence of the luminous-lens effects on the centroidal shifts (and light curve) on top of a FSFL event in Fig. 8. Since the limb-darkening only slightly modifies the trajectory as shown in Fig. 6, we demonstrate the luminous-lens effects in the FSFL regime assuming a uniform brightness source in Fig. 8. We show the luminous-lens effects with various values for an apparent magnitude difference between the lens and source

$$\Delta m_{LS} = m_L - m_S = -2.5 \log_{10}(f_{LS}). \quad (17)$$

For illustrational purpose, we show the luminous-lens effects on top of the FSFL for different sizes of the lens and the source in Fig. 9. When the lens is getting brighter, the trajectory becomes smaller and rounder. The signal of centroidal shift is thus reduced for a source blended by a luminous lens. The case of a PSPL events with luminous lens in Fig. 9 (upper left-hand corner) is comparable to the results of Jeong, Han, & Park (1999). Note that for the PSFL when $\rho_L = 1.3$ (lower left-hand corner), the trajectory vanishes when $\rho_L > \theta_+$ for the dark lens case (black dotted line), but follows the trajectory of the lens for luminous-lens cases.

Since equation (16) gives us the full consideration of the FSFL effects with the brightness of the source and lens (note that we only need to consider the flux ratio between the lens and the source, so the limb-darkening effects of the lens does not need to be taken into account), one is able to derive the information of ρ_S , Γ_S , ρ_L , and f_{LS} by fitting the centroidal shifts. In principle, one can fit both the centroidal shifts and the light curve, to utilize both the astrometric and photometric information and thus to have a better constrain on the events parameters in equation (16). Once the aforementioned

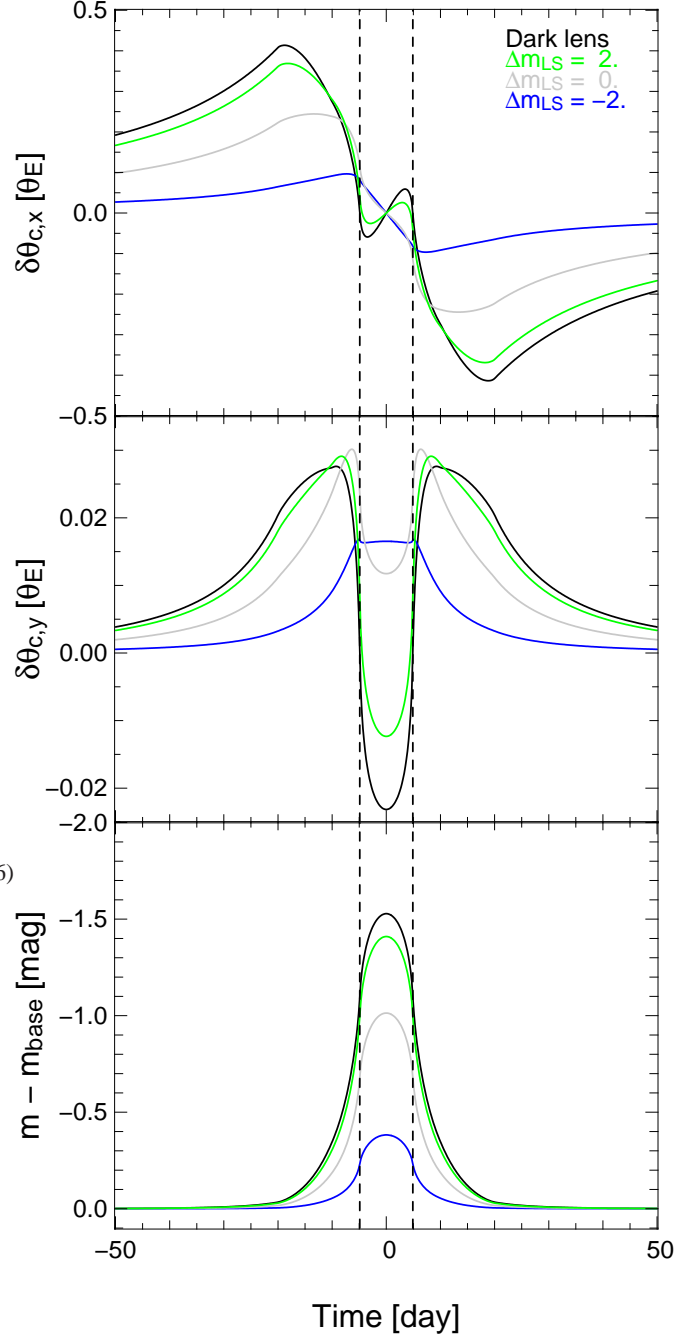


Figure 8. Centroidal shifts decomposition and light curves of a microlensing event assuming $u_0 = 0.1 \theta_E$, source radius $= 0.5 \theta_E$ and lens radius $= 0.5 \theta_E$. We show the trajectory in the x- and y-direction (as in Fig. 1) of a bright lens with $\Delta m_{LS} = -2$ (in blue), 0 (in gray), 2 (in green) and with a dark lens (in black). We also show the light curve with the magnitude variation relative to the baseline (m_{base}). The vertical dashed line indicates the time when $u_0 = \rho_S$.

parameters are all well determined, we can use the value of θ_E to derive both the size of the lens and the source. We can also derive the mass of the lens as shown in equation (2) given the information of the microlens parallax π_E . The distance to the lens is also available if the distance to the source is well known, e.g. if the source is located in the Galactic bulge or Magellanic Clouds, which is often the case for the current microlensing surveys. In these cases, we are

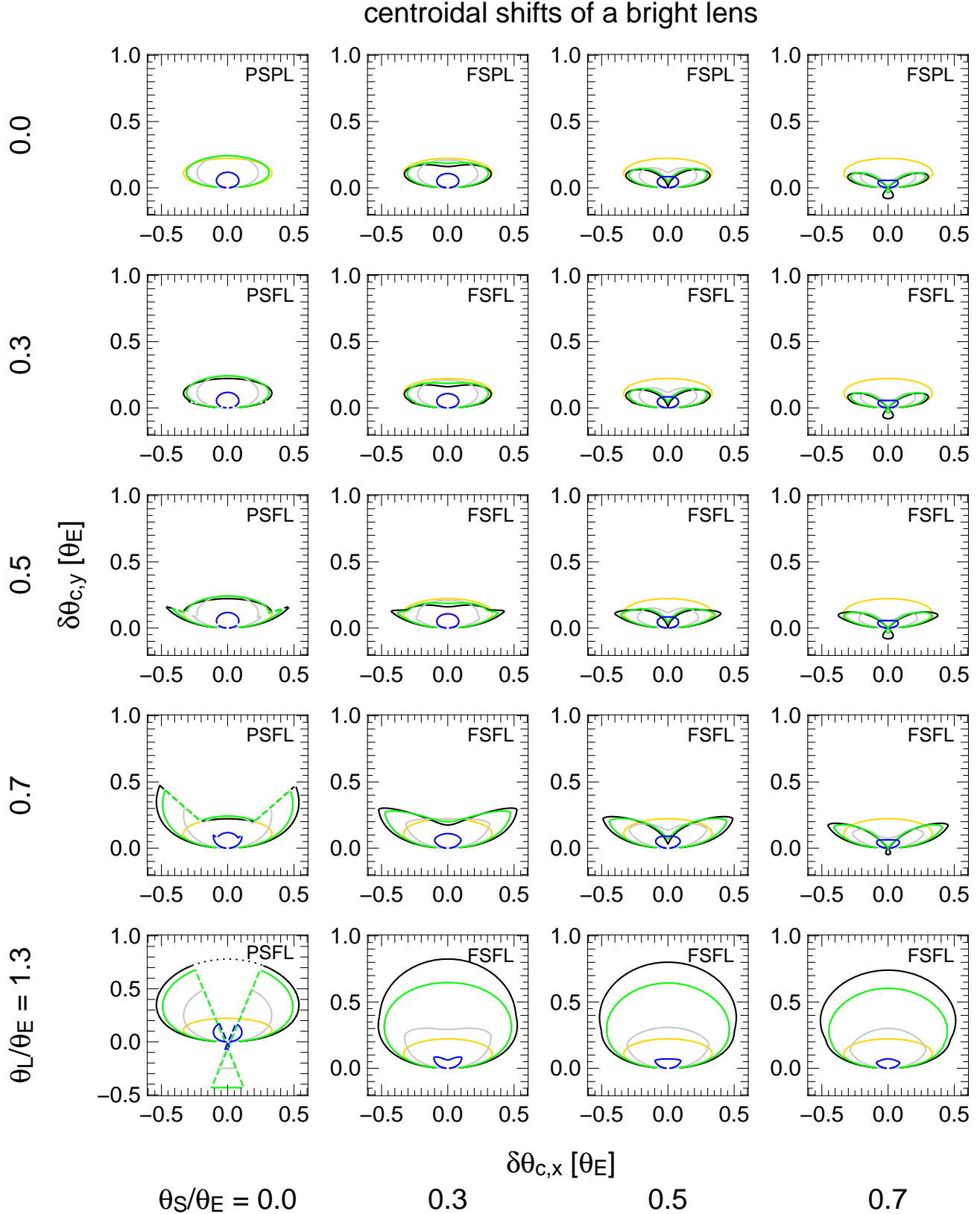


Figure 9. Centroid shifts in the presence of FS and FL effects for a luminous lens. We show the examples for a PSPL (in yellow), FSFL with $\Delta m_{LS} = -2$ (in blue), 0 (in gray), 2 (in green) and with a dark lens (in black) assuming $u_0 = 0.5 \theta_E$ and with the sizes of the source and the lens varying from $0.3 \theta_E$ to $1.3 \theta_E$. The dashed lines in the plots with $\theta_S/\theta_E = 0.0$ show the discontinuity in the trajectories for the PSFL cases. The dotted lines in the PSFL with $\theta_L/\theta_E = 1.3$ indicates the trajectory when the lens totally obscures both the plus- and minus-image.

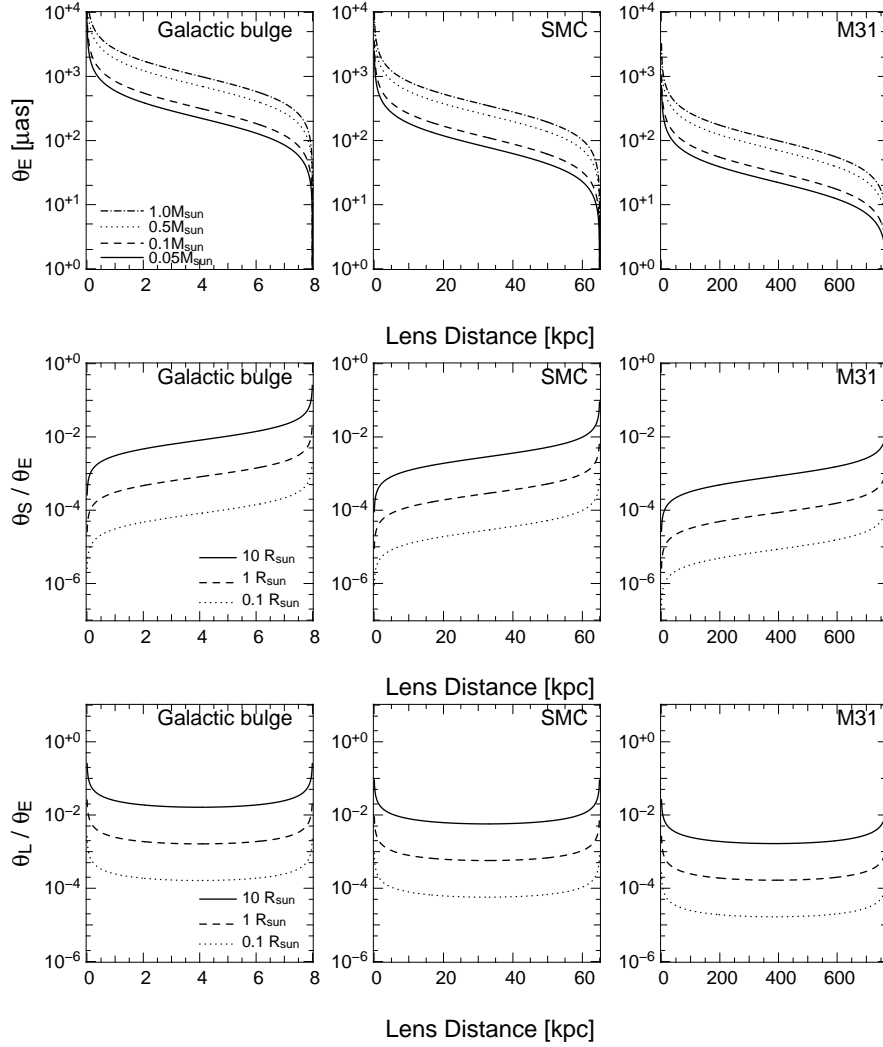


Figure 10. First row: θ_E as a function of D_{OL} assuming the source located in the Galactic bulge ($D_{OS} = 8$ kpc), SMC ($D_{OS} = 65$ kpc), and M31 ($D_{OS} = 770$ kpc). Second and third row: θ_S/θ_E and θ_L/θ_E as a function of the lens distance assuming $M_L = 0.5M_\odot$.

able to estimate the physical parameters of the whole microlensing systems.

6 OBSERVATIONAL FEASIBILITY

In this section we consider the astrometric events towards the Galactic bulge, SMC and M31 assuming $D_{OS} = 8$, 65, and 770 kpc, respectively. We substitute $D_{OL}/D_{OS} = x$ into equation (1), which then becomes

$$\theta_E = \sqrt{\frac{4GM_L}{c^2 D_{OS}} \left(\frac{1}{x} - 1 \right)}. \quad (18)$$

Therefore, θ_E is smaller for a source located at larger distance and is smaller for larger lens distance given the same source location (see upper panels in Fig. 10).

Equation (18) also implies that the halo lensing events have larger Einstein radii than self-lensing events for a given lens mass. For instance, halo lensing events towards SMC with $D_{OL} = 15$ kpc and $M_L = 1 M_\odot$ will induce an astrometric signal with $\theta_E = 645 \mu\text{as}$, which is one order of magnitude larger than for self-lensing

events ($44 \mu\text{as}$ at $D_{OL} = 64$ kpc). Thus we are able to distinguish halo and self-lensing events by the size of the astrometric ellipse.

The FS effects play an important role when $u_0 \leq \rho_S$, which is often the case when $u_0 \ll 1$ (Gould 1994). However, such a configuration leads to a smaller centroidal shift (as shown in Fig. 1) and is thus very challenging to distinguish between the PSPL and FSPL trajectories observationally.

FL effects are prominent when ρ_L is close to and larger than unity (as shown in Fig. 7). We thus calculate ρ_L by dividing the angular lens radius θ_L by θ_E (see the lower panel in Fig. 10). Because θ_L is proportional to $1/x$ while θ_E is a function of $\sqrt{1/x - 1}$, ρ_L is actually a function of $[x(1 - x)]^{-1/2}$. We would expect to see the FL effects when the lens is located either close to the observer ($x \approx 0$) or to the source ($x \approx 1$). By equating θ_L to θ_E , we have

$$\frac{D_{OL}}{D_{OS}} (D_{OS} - D_{OL}) = \frac{R_L^2 c^2}{4GM_L}. \quad (19)$$

The left-hand side of this equation gives us the information on the location of the lens to have prominent FL effects (Agol 2002). If the lens is very close to the observer such that $D_{OL} \ll D_{OS}$, equation (19) gives us an upper limit of D_{OL} so that for lenses be-

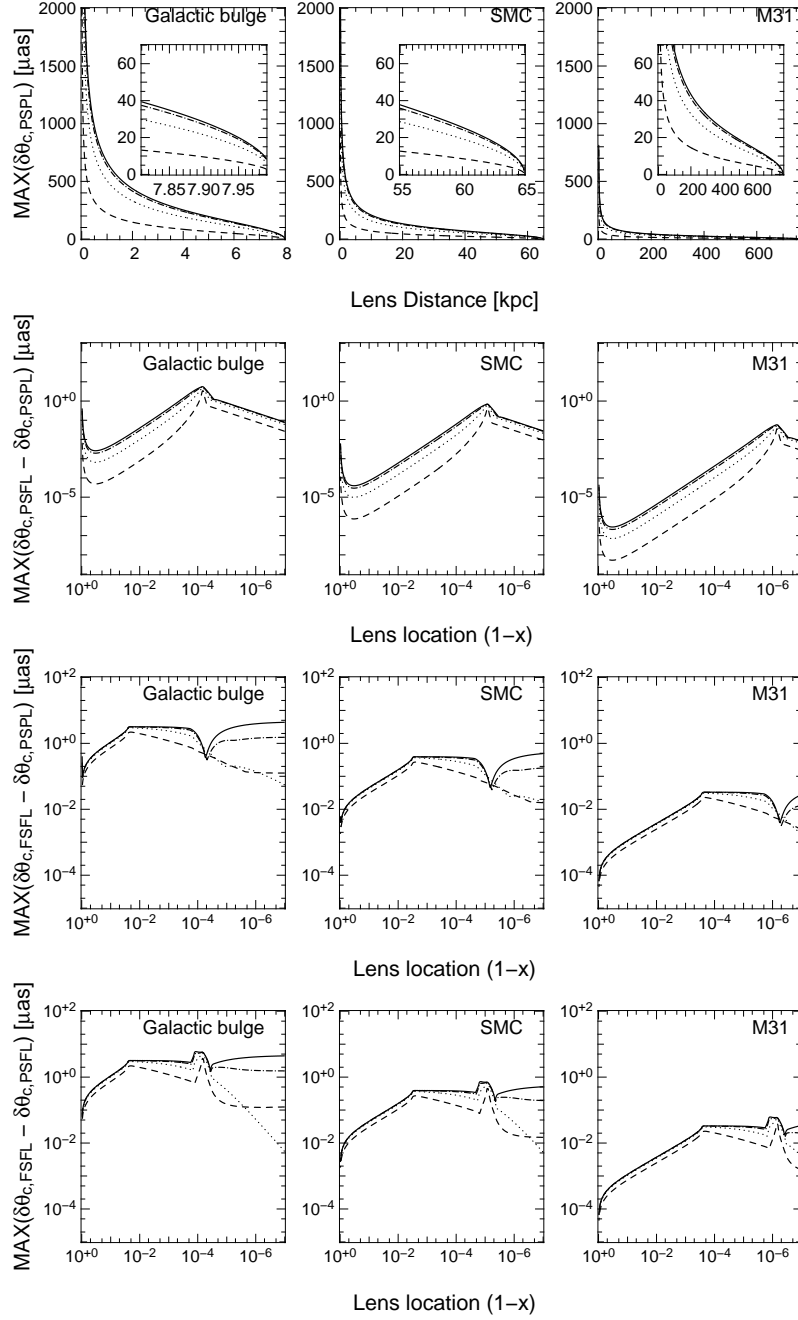


Figure 11. First row: maximum centroidal shifts as a function of D_{OL} assuming the source located in the Galactic bulge ($D_{OS} = 8$ kpc), SMC ($D_{OS} = 65$ kpc), and M31 ($D_{OS} = 770$ kpc) in PSPL. Second row: maximum deviation between the PSFL and PSPL trajectories as a function of the lens location $(1-x)$, where $x = D_{OL}/D_{OS}$. Third row: maximum deviation between the FSFL and PSPL trajectories. Fourth row: maximum deviation between the FSFL and PSFL trajectories. We assume $u_0 = 0.05 \theta_E$, $t_E = 10$ days, $M_L = 0.5 M_\odot$, $R_L = 10 R_\odot$, and $R_S = 10 R_\odot$. Here we show the cases of a luminous lens with $\Delta m_{LS} = 2$ (in dashed), 0 (in dotted), -2 (in dash-dotted), and a dark lens (in solid).

yond this value, the FL effect is not prominent. On the other hand, if the lens is very close to the source so that $D_{OL} \approx D_{OS}$, then equation (19) actually gives us a maximum separation between the lens and the source in order to have non-negligible FL effects. The value of $D_{OL}(D_{OS} - D_{OL})/D_{OS}$ for several astrophysical objects are given in Table 1.

We then calculate the maximum centroid deviation versus lens distance for the cases of PSPL, PSFL, FSPL, and FSFL assuming that a source of $10 R_\odot$ is amplified by a lens of $0.5 M_\odot$ and $10 R_\odot$ with the minimum lens-source separation projected onto the sky

to be $0.05 \theta_E$. Because there are only small differences between PSPL, PSFL, FSPL, and FSFL, we only show the case of PSPL in Fig. 11. To see how much the FL trajectory deviates from that of PL and the influence from FS, we further calculate the maximum difference between the PSPL, PSFL, and FSFL trajectories at a given time. The result is shown in Fig. 11 for a lens with $\Delta m_{LS} = 2, 0, -2$ and a dark lens. The FSFL only shows small difference to that of PSFL and PSPL. The difference is less than $10 \mu\text{as}$ for the case of Galactic bulge, and even smaller than $1 \mu\text{as}$ for the more distant source in the SMC and M31. This is because the FL effect

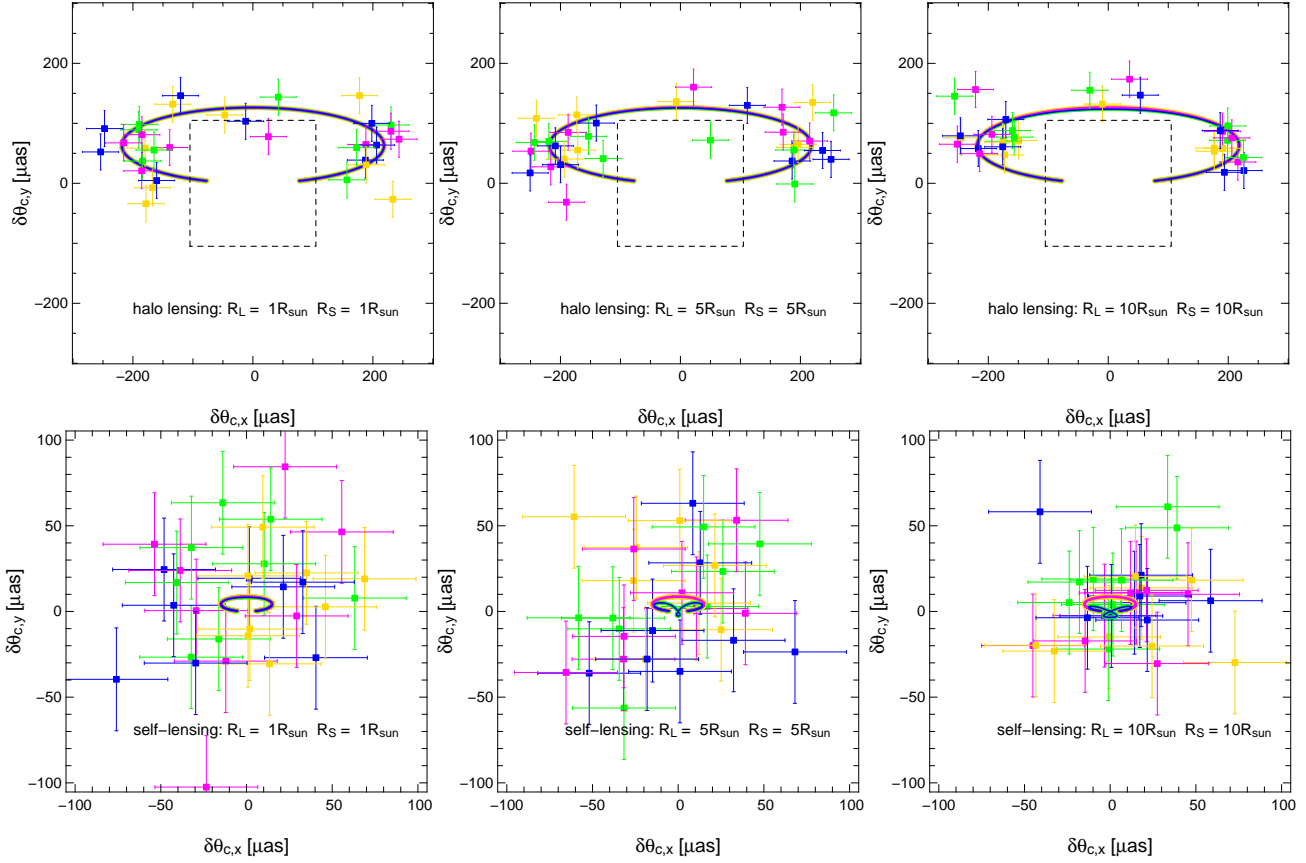


Figure 12. Astrometric trajectory of the SMC microlensing event MACHO-97-SMC-1 with $t_E = 123.5$ days and $u_0 = 0.426824 \theta_E$. We show the case when the lens is located in the Galactic halo (upper panels) and in SMC (lower panels). We assume the lens is $1 M_\odot$ and the size of the lens and the source are assumed to be 1, 5, and $10 R_\odot$, respectively. The color convention is the same as Fig. 4. We calculate the theoretical trajectory within a time interval of $t_0 \pm 1000$ days. We then simulate the measurements of *SIM*, with a sampling rate of every 90 days spanning for $t_0 \pm 1$ year and $30\text{-}\mu\text{as}$ error in both x and y directions. The dashed square in the halo lensing cases outlines the dimension showed in the self-lensing regime.

Table 1. $D_{OL}(D_{OS} - D_{OL})/D_{OS}$ for several astrophysical objects.

Name	Radius (R_\odot)	Mass (M_\odot)	$\frac{D_{OL}}{D_{OS}}(D_{OS} - D_{OL})$
Sun	1.	1.	551 AU
Jupiter	0.1	0.001	5.5×10^3 AU
Earth	0.009	3×10^{-6}	1.5×10^4 AU
Brown dwarf	0.1	0.05	110 AU
White dwarf	0.009	1.	0.045 AU
Neutron star	2.8×10^{-5}	1.4	3.1×10^{-7} AU
Black hole	4.2×10^{-5}	10.	9.9×10^{-8} AU
Test case	10.	0.5	1.1×10^5 AU

is important only when the lens is extremely close to the observer or the source and the major difference between FSFL and PSPL or PSFL comes from the finiteness of the source. Since u_0 is larger than ρ_s for most of the time, the FS effect only slightly changes the astrometric trajectory. Even when the lens is extremely close to the source (see Fig. 11), the already reduced θ_E makes the difference so small that it is hardly observable.

In order to test if the astrometric signal is observable towards SMC, we simulate the astrometric trajectory of MACHO-97-SMC-1 (Alcock et al. 1997a). This event has baseline magnitude $V = 17.7$, so it will take *SIM* ~ 3 hours to reach $30\text{-}\mu\text{as}$ accuracy (Goullioud et al. 2008). We thus simulate observations by *SIM* as-

suming the measurement errors to be Gaussian distribution with $\sigma = 30 \mu\text{as}$. We put the lens at a distance of 15 kpc and 64 kpc corresponding to the halo and self-lensing scenario towards SMC. We then assign a putative finite size of 1, 5, and $10 R_\odot$ to the lens and the source. The mass of the lens is set to be $1 M_\odot$. From Fig. 12 we can see that if the lens is in the Galactic halo, we are able to detect the astrometric signal because of the very large θ_E . However, the finite size of the source and the lens is not revealed in such a close lens. On the other hand, the FS and FL effects are prominent in the self-lensing regime due to the small θ_E . But the astrometric trajectory is too small to be constrained by current instruments, not to mention to disentangle between the PSPL and FSPL or PSFL. Nevertheless, it is still possible to use the (non-)detection of the astrometric ellipse to infer if the lens is in the Galactic halo or it is a self-lensing event towards SMC.

We also considered the possibility to detect the astrometric trajectory from ground-based instruments such as *PRIMA* for VLTI. *PRIMA* can determine the astrometry to $10\text{-}\mu\text{as}$ level in 30 minutes provided a reference star within 10 arcsec and a 200-m baseline (ATs mode). The goal of *PRIMA* is to perform astrometric measurement for a target as faint as 18 (15) mag with UTs (ATs) provided a 13 (10) mag reference star in *K* band (Delplancke 2008). There is a bright star ($K = 10.28$) in the vicinity of MACHO-97-SMC-1 (separated at 30.4 arcsec), so theoretically it would be possible to obtain $30\text{-}\mu\text{as}$ accuracy in astrometric measurements within one

hour with the UTs (130 m baseline). However, for the two stars separated by 20 arcsec, there is already 90% reduction in the interferometric fringe visibility. Thus it would be very challenging to conduct such measurement. It would be very difficult to routinely measure the astrometry towards SMC/LMC with *PRIMA* because most of the single lens events in the Magellanic Clouds (14 out of 15, except MACHO-97-SMC-1) have sources fainter than 19 mag in *V* (1 in Alcock et al. 1997a; 12 in Alcock et al. 2000; 1 in Tisserand et al. 2007, which is the same as Alcock et al. 1997a, and 2 in Wyrzykowski et al. 2009).

To perform astrometric measurements for microlensing events towards M31 is beyond the limit of both *PRIMA* and *SIM* since the sources in M31 are too faint (see e.g. Riffeser et al., in preparation, and reference therein).

7 CONCLUSION

We have studied the astrometric aspects of microlensing by simultaneously including the FS and FL effects. Our results show that the astrometric signal is underestimated or overestimated by assuming PL or PS, respectively. While the FS effect is prominent when the lens transits the surface of the source, the FL effect is revealed when the lens is very close to the source, which would be in the self-lensing regime. In the context of the self-lensing scenario, where a background star is lensed by a foreground star, the light contribution from the lens is in general not negligible. We thus consider the luminous-lens scenario, which attenuates the signal of the centroidal displacement. Astrometric trajectories with a source located in the Galactic bulge, SMC, and M31 are discussed, which show that θ_E of halo-lensing events is at least one order of magnitude larger than that of self-lensing in SMC and M31. Our results also indicate that the finiteness of the lens is more likely to be revealed in the self-lensing scenario towards distant source located in Magellanic Clouds or M31, although it is very difficult to distinguish between PL and FL with current instruments.

ACKNOWLEDGMENTS

We are very grateful to the anonymous referee for the useful comments. This work was supported by the DFG cluster of excellence ‘Origin and Structure of the Universe’ (www.universe-cluster.de).

REFERENCES

- Agol E., 2002, *ApJ*, 579, 430
 Albrow M. D., et al., 2000, *ApJ*, 534, 894
 Alcock C., et al., 1997a, *ApJ*, 491, L11
 Alcock C., et al., 1997b, *ApJ*, 491, 436
 Alcock C., et al., 2000, *ApJ*, 542, 281
 Alcock C., et al., 2001, *Natur*, 414, 617
 Allen R. J., Peterson D. M., Shao M., 1997, *SPIE*, 2871, 504
 Batista V., et al., 2009, *A&A*, 508, 467
 Belokurov V. A., Evans N. W., 2002, *MNRAS*, 331, 649
 Boden A. F., Shao M., van Buren D., 1998, *ApJ*, 502, 538
 Cassan A., et al., 2006, *A&A*, 460, 277
 Delplancke F., 2008, *NewAR*, 52, 199
 Dominik M., Sahu K. C., 2000, *ApJ*, 534, 213
 Fouqué P., et al., 2010, *A&A*, 518, A51
 Gould A., 1992, *ApJ*, 392, 442
 Gould A., 1994, *ApJ*, 421, L71
 Gould A., 2000, *ApJ*, 542, 785
 Goullioud R., Catanzarite J. H., Dekens F. G., Shao M., Marr J. C., IV, 2008, *SPIE*, 7013,
 Hog E., Novikov I. D., Polnarev A. G., 1995, *A&A*, 294, 287
 Hosokawa M., Ohnishi K., Fukushima T., Takeuti M., 1993, *A&A*, 278, L27
 Jeong Y., Han C., Park S.-H., 1999, *ApJ*, 511, 569
 Jiang G., et al., 2004, *ApJ*, 617, 1307
 Kozłowski S., Woźniak P. R., Mao S., Wood A., 2007, *ApJ*, 671, 420
 Alcock C., Werner M. W., Fazio G. G., 2006, *ApJ*, 652, L97
 Lee C.-H., Riffeser A., Seitz S., Bender R., 2009, *ApJ*, 695, 200
 Lindegren L., et al., 1994, *SPIE*, 2200, 599
 Mao S., Witt H. J., 1998, *MNRAS*, 300, 1041
 Miyamoto M., Yoshii Y., 1995, *AJ*, 110, 1427
 Quirrenbach A., et al., 1998, *SPIE*, 3350, 807
 Takahashi R., 2003, *ApJ*, 595, 418
 Tisserand P., et al., 2007, *A&A*, 469, 387
 Walker M. A., 1995, *ApJ*, 453, 37
 Wyrzykowski Ł., et al., 2009, *MNRAS*, 397, 1228
 Yee J. C., et al., 2009, *ApJ*, 703, 2082
 Yoo J., et al., 2004, *ApJ*, 603, 139
 Zub M., et al., 2009, *arXiv*, arXiv:0912.2312